

Multiband tight-binding approach to tunneling in semiconductor heterostructures: Application to ΓX transfer in GaAs

J. A. Støvneng*

NORDITA, Blegdamsvej 17, DK-2100 Copenhagen Ø, Denmark

P. Lipavský

Institute of Physics, Academy of Sciences of Czech Republic, Na Slovance 2, 18040 Praha 8, Czech Republic

(Received 2 August 1993)

We study tunneling in semiconductor heterostructures where the constituent materials can have a direct or an indirect band gap. In order to have a good description of the lowest conduction band, we have used the nearest-neighbor sp^3s^* tight-binding model put forward by P. Vogl *et al.* A recursive Green-function method yields transmission coefficients from which an expression for the current density may be written down. The method is applied to GaAs/AlAs heterostructures. Electrons may traverse the AlAs barriers via different tunneling states ψ_Γ and ψ_X (ΓX mixing). With an applied bias $V \gtrsim 0.5$ V electrons may enter the GaAs collector contact in both the Γ and the X valleys (ΓX transfer). We have studied a number of GaAs/AlAs structures. For very narrow barriers there is little ΓX transfer, but AlAs barriers wider than about 25 Å act as “ ΓX filters,” i.e., most transmitted electrons have been transferred to the X valley.

I. INTRODUCTION

Tunneling in semiconductor heterostructures has attracted considerable interest over the last decade. A very important motivation factor has been the progress in advanced crystal-growth techniques such as molecular-beam epitaxy. The ability to grow nearly perfect layered structures has enabled experimental verification of predictions based on relatively simple theoretical models. There is also a great interest in making electronic devices based on such structures.

Most treatments of transport through heterostructures have been based on effective-mass theory. This is a good approximation when the different materials that form the structure all belong to the same category with respect to type of energy band gap, *direct* or *indirect*. An example of a system with only direct-band-gap constituents is GaAs/Al_xGa_{1-x}As, provided the Al concentration is sufficiently low, $x \lesssim 0.4$. In a typical experiment, doping in the GaAs contacts yields a Fermi level E_F of the order of 10–50 meV above the conduction-band minimum E_c^Γ at the Γ point of the Brillouin zone ($\mathbf{k}=0$). Since the conduction band is nearly parabolic in the range from E_c^Γ to E_F , all the incoming electrons are well described by a single effective mass $m_\Gamma^*(\text{GaAs})$. Furthermore, the lowest tunneling barrier is determined by the conduction-band minimum in Al_xGa_{1-x}As, which is also at the Γ point. Thus the *tunneling states*, through which electrons with energy E can traverse the barrier region, are characterized by an imaginary wave vector $k = i\kappa$, where κ is determined by the tunneling-barrier height $E_c^\Gamma(\text{Al}_x\text{Ga}_{1-x}\text{As}) - E$ and the effective mass $m_\Gamma^*(\text{Al}_x\text{Ga}_{1-x}\text{As})$.

For Al concentrations $x > 0.4$, Al_xGa_{1-x}As becomes an indirect-band-gap material. The valence-band maximum is still at the Γ point, but the conduction-band

minimum is now E_c^X , close to the X point, $\mathbf{k} = 2\pi/a_L(100)$, at the edge of the Brillouin zone. Here a_L is the lattice constant of the zinc-blende material. When indirect-band-gap Al_xGa_{1-x}As is used as the barrier material, it is no longer sufficient to take into account only the tunneling states that correspond to the conduction-band minimum at Γ . Also important are the states that correspond to the analytical continuation into the energy gap of real- \mathbf{k} states at the conduction-band minimum near the X point. “ Γ states” and “ X states” may have comparable decay lengths since the lower barrier height of the X states, $E_c^X - E$, is compensated for by a higher effective mass. The importance of X states in tunneling through indirect-band-gap barriers has already been appreciated in several experiments^{1–10} and it has also been studied theoretically by a number of groups.^{11–18}

In the present paper, we want to focus on the X states in *both* the barrier and the contact material. It is well known that electrons in bulk GaAs may be transferred from the Γ to the L or X valleys if they are accelerated in a sufficiently strong electric field. This is the Gunn effect which may be accompanied by a region of negative differential conductivity in the current-voltage curve due to the low mobility of electrons in the satellite valleys. The “ ΓX (ΓL) transfer” is usually stimulated by some kind of scattering mechanism, e.g., elastic-impurity scattering. Our aim is to show how a heterostructure with one or more indirect-band-gap barriers can be used to control the ΓX transfer in a material like GaAs. Let us assume that the transport takes place in the (100) direction. Then, with a bias $V > [E_c^X(\text{GaAs}) - E_F]/e$ applied across the heterostructure, incoming electrons in the left contact can end up in two final states in the right contact, in the Γ valley or in the X valley. The two outcomes are characterized by transmission coefficients T_Γ and T_X , respectively, which depend on the energy of in-

coming electrons, applied bias, and barrier parameters. In Sec. V below, we shall explore these dependencies for GaAs/AlAs heterostructures in order to find effective “ ΓX filters,” i.e., conditions under which $T_X \gg T_\Gamma$.

In transport experiments the measured quantity is usually the electric current vs the applied voltage. Based on simple arguments one can write down an expression for the current density in terms of transmission coefficients and a factor ensuring that initial states are occupied and final states are empty. In the present case a sum over different final states at equal energy automatically provides a decomposition of the current density in a “direct” component J_Γ and a “transferred” one J_X . This simple procedure is indeed applicable in the present study of perfectly layered heterostructures where we ignore effects of disorder and inelastic scattering. If such effects are to be included, one must resort to a more general approach. In an Appendix, we derive an expression for the current density which provides the starting point for extensions to more realistic calculations.¹⁹ The general expression involves nonequilibrium Green functions and gives the *total* current density J , *not* the decomposition into J_Γ and J_X . However, in the case where disorder and phonons can be ignored, we will show how the general expression for $J(V)$ can be decomposed and proven to be identical to the result which was written down directly in terms of transmission probabilities.

The transmitted electrons will be subject to elastic and inelastic scattering and eventually come to thermal equilibrium somewhere in the right contact. This process may be described by scattering rates $\tau_{\Gamma\Gamma}^{-1}$, τ_{XX}^{-1} , and $\tau_{X\Gamma}^{-1}$, where the former two account for intravalley scattering and the latter describes the relaxation of X electrons to the Γ valley. Clearly, $\tau_{X\Gamma}$ sets the time scale for observing or taking direct advantage of having electrons in the X valley.

The rates of elastic and inelastic scattering depend mainly on impurity concentration and temperature, respectively. At low temperatures the dominating inelastic process in GaAs is spontaneous emission of LO phonons. A rough estimate, based on Refs. 20–22, yields an inelastic relaxation rate on the order of 10^{13} s^{-1} in both the Γ and the X valley. A similar estimate yields an *intervalley* scattering rate $\tau_{X\Gamma}^{-1} \sim 10^{12} \text{ s}^{-1}$, taking into account that electrons in the X valley may relax to the Γ valley via emission of LO phonons or via scattering off charged impurities (assuming impurity concentrations of about 10^{17} cm^{-3}). This implies that, with an average drift velocity of about 10^5 m/s , a transferred electron travels typically a distance of 1000 Å in the X valley.

One way of detecting X electrons, then, could be by means of a magnetic field B applied parallel to the crystal-growth direction, and taking advantage of the difference in Landau-level splitting ($\Delta E_{LL} = \hbar\omega_c = \hbar eB/m^*$) in the Γ and the X valley due to the difference in effective mass ($m_X^* \gg m_\Gamma^*$). However, in order to test predictions for the ΓX transfer, it may even, for carefully designed heterostructures, be sufficient to measure the *total* current vs the applied voltage. If the nonlinear structure in the measured total current is well described by the theory, it seems reasonable to assume

that the calculated decomposition into J_Γ and J_X also agrees with reality. Finally, the ΓX transfer may be checked by investigating the noise spectrum of the current. Quite often the noise spectrum of a given physical quantity may reveal sharper features and more information than a measurement of the physical quantity itself.²³

The effects we want to study involve states far from the local minima of the conduction band and also states in more than one valley. In order to describe the band structure correctly, at least qualitatively, we apply the semiempirical sp^3s^* tight-binding (TB) Hamiltonian put forward by Vogl *et al.*²⁴ A feature of this model, of particular interest here, is the correct description of the transition in $\text{Al}_x\text{Ga}_{1-x}\text{As}$ from a direct to an indirect band gap. In addition, it is a three-dimensional model which makes it suitable for evaluation of current-voltage characteristics. The sp^3s^* model was also used by Cade *et al.*¹¹ and by Yamaguchi.²⁵

We have organized the paper as follows. In Sec. II we describe briefly the sp^3s^* TB Hamiltonian. In Sec. III we derive expressions for the scattering coefficients. An expression for the current density is presented in Sec. IV, and in Sec. V we perform a systematic study of the ΓX transfer in GaAs/AlAs heterostructures. We conclude in Sec. VI and discuss briefly possible extensions and other applications of the present model.

II. THE sp^3s^* HAMILTONIAN

The semiconductors that we want to describe have the crystal structure of zinc blende. The *valence bands* of these materials are usually well described by an eight-band sp^3 nearest-neighbor semiempirical TB Hamiltonian,^{24,26} the eight bands arising from the inclusion of four atomic orbitals on each of the two types of atoms, cation and anion. However, for electronic transport and tunneling we need a model that describes the *lowest conduction bands* adequately, and for that purpose the nearest-neighbor sp^3 model generally fails. In particular, as shown by Chadi and Cohen,²⁷ it cannot produce an indirect band gap in materials like AlAs, and this is the single most important feature required for our purposes.

Vogl *et al.*²⁴ have overcome this deficiency by the *ad hoc* inclusion of an excited s^* state on each atom. The main effect of coupling these s^* states to nearest-neighbor p states is to repel the p -like conduction-band levels near the X and L points to lower energies, thus producing the desired indirect band gap. The resulting ten-band sp^3s^* Hamiltonian has thirteen independent TB matrix elements that are determined by fitting band-structure data.

The independent TB matrix elements are given in a basis of symmetrically orthogonalized atomic orbitals $|nb\mathbf{R}\rangle$, also called Löwdin orbitals.²⁸ Here \mathbf{R} is the position of the atom, n denotes the type of orbital (s , p , or s^*) and b the type of atom (c for cation and a for anion). In Ref. 24 the Hamiltonian for bulk material is expressed as a 10×10 matrix in a basis $|nb\mathbf{k}\rangle$ which is obtained by a discrete Fourier transform of the localized orbitals $|nb\mathbf{R}\rangle$. The systems that we want to study are translationally invariant in the “parallel” plane (y, z). However,

the heterostructure breaks the invariance in the crystal-growth direction, which is usually chosen to be along the (100) axis. Thus it is convenient to represent the Hamiltonian in a basis $|nbj\mathbf{k}_\parallel\rangle$ with parallel momentum $\mathbf{k}_\parallel=(k_y, k_z)$ and “perpendicular” position $x_j=ja_L/4$ as parameters. The distance between nearest-neighbor planes is one fourth the lattice constant a_L . A simple inverse Fourier transform (with the same normalization convention as in Ref. 24),

$$|nbj\mathbf{k}_\parallel\rangle=L_{\text{BZ}}^{-1/2}\int dk_x e^{-ik_x ja_L/4}|nb\mathbf{k}\rangle, \quad (2.1)$$

yields the desired basis. Here $L_{\text{BZ}}=8\pi/a_L$ is the length of the one-dimensional (1D) Brillouin zone over which the k_x integral is taken.

In the new basis the Hamiltonian takes the form

$$H=\begin{bmatrix} \ddots & \ddots \\ & V_{ca} & E_c & U_{ca} & & & & & & \\ & U_{ac} & E_a & V_{ac} & & & & & & \\ & & V_{ca} & E_c & U_{ca} & & & & & \\ & & U_{ac} & E_a & V_{ac} & & & & & \\ & & & \ddots \end{bmatrix}, \quad (2.2)$$

where each element is a 5×5 matrix. The matrices E_c and E_a are diagonal and represent the orbital energies on cations and anions, respectively, whereas the “hopping” terms U_{ca} , U_{ac} , V_{ca} , and V_{ac} involve the various transfer-matrix elements between orbitals on neighboring sites. Obviously $U_{ac}=U_{ca}^\dagger$ and $V_{ac}=V_{ca}^\dagger$ so that the Hamiltonian is Hermitian. In Appendix A the elements of H are given in detail, and we have also included the numerical values of the matrix elements for GaAs and AlAs, taken from Ref. 24. The Hamiltonian in Eq. (2.2) is formally identical to that of a two-atomic 1D chain with interatomic separation $a_L/4$ and periodicity $a_L/2$, see Fig. 1.

Alloys will not be treated explicitly in the present paper. We only mention that the simplest approach would be the virtual-crystal approximation (VCA). This means that the Hamiltonian of an alloy $A_x B_{1-x} C$ is approximated by the weighted average of the Hamiltonians of AC and BC , e.g., $U_{ca}[A_x B_{1-x} C]=xU_{ca}[AC]+(1-x)U_{ca}[BC]$. Scattering due to disorder in the cation planes is neglected in the VCA. That effect can be included by replacing VCA with the so-called coherent-potential approximation.

Another effect that is ignored in this work, is elastic scattering due to interface roughness. Like alloy disorder, interface roughness breaks the translational invariance in the parallel plane. Hence the parallel momentum is no longer conserved, and the simple treatment of the next section must be modified. Interface-roughness scattering can also be accounted for within the coherent-potential approximation.

To summarize this section, we use a model which basically extends the simplest models of tunneling by incorporating a semirealistic band structure. All other approximations are still included, e.g., neglect of inelastic scattering, disorder, and many-particle effects.

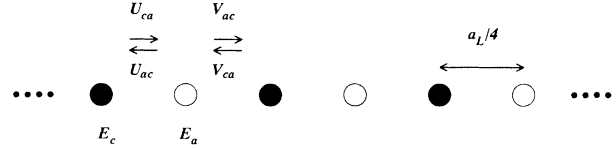


FIG. 1. Projection of the zinc-blende lattice on the (100) direction. Closed and open circles represent cation and anion layers, respectively. The interlayer distance is $a_L/4$, i.e., one fourth the lattice constant. Indicated are also the “on-layer” energies E_c and E_a , and the interlayer hopping matrices U_{ca} , U_{ac} , V_{ca} , and V_{ac} .

III. SCATTERING COEFFICIENTS

When the physical system is described with an effectively 1D nearest-neighbor TB Hamiltonian, the scattering states can be evaluated efficiently with a recursive Green-function technique. This method has been applied to various problems.²⁹ The present treatment will essentially be a generalization of the simple one-band 1D chain described in detail in Ref. 30.

Since we will discuss only processes where the parallel momentum \mathbf{k}_\parallel is conserved, we will suppress \mathbf{k}_\parallel in most of the notation of this section. It is, furthermore, convenient to label a cation layer and its neighboring anion layer to the right with a common “site” index j . Assume that the heterostructure and the undoped spacer layers, if any, are located on the sites from $j=1$ to $j=N$. Then the homogeneous “leads” extend from $j=-\infty$ to $j=0$ and from $j=N+1$ to $j=\infty$. Write the total wave function $|\Psi\rangle$ as a sum of two pieces,

$$|\Psi\rangle=|S_\alpha\rangle+|\phi\rangle. \quad (3.1)$$

The first term is taken to be the incoming plane-wave part with wave number $\mathbf{k}_\alpha=(k_\alpha, \mathbf{k}_\parallel)$ and energy E , restricted to layers up to and including the cation part of site 0:

$$|S_\alpha\rangle=\sum_{j\leq 0, c} e^{ik_\alpha ja_L/2}|j, \alpha\rangle. \quad (3.2)$$

The local part $|j, \alpha\rangle$ is a 10×1 vector with coefficients α_{nb} ($n=s, p_x, p_y, p_z, s^*$ and $b=c, a$). These coefficients are determined by the solution of the Schrödinger equation for the bulk material at energy E and wave vector \mathbf{k}_α . The problem is now reduced to finding the “remainder” $|\phi\rangle$, and since $(E-H)|\Psi\rangle=0$, we have

$$|\phi\rangle=G^R(E)[-(E-H)|S_\alpha\rangle]. \quad (3.3)$$

Here $G^R(E)=\lim_{\eta\rightarrow 0^+}(E-H+i\eta)^{-1}$ is the retarded Green function which also depends on \mathbf{k}_\parallel via the Hamiltonian. From the definition (3.2) of $|S_\alpha\rangle$, and since H only couples nearest-neighbor atomic layers, the term in square brackets in (3.3) is clearly zero for sites $j>0$. Furthermore, the Schrödinger equation ensures that $(E-H)|S_\alpha\rangle=0$ for sites $j<0$, and one is left with nonzero terms only on the cation and anion layer at site $j=0$. We may finally write

$$|\phi\rangle=\frac{4i\hbar}{a_L}G^R(E)\hat{v}|0, \alpha\rangle, \quad (3.4)$$

where \hat{v} resulting from (3.3) reads

$$\hat{v} = \frac{a_L}{4\hbar} \begin{bmatrix} 0 & iU_{ca} \\ -iU_{ac} & 0 \end{bmatrix}. \quad (3.5)$$

The operator \hat{v} can be interpreted as a local velocity operator. This is consistent with the velocity operator obtained from the Heisenberg equation of motion, $\hat{v} = -i/\hbar[\hat{x}, H]$, with the position operator

$$|\Psi\rangle = \sum_{j \leq 0} \left[e^{ik_a j a_L / 2} |j, \alpha\rangle + \sum_{\beta} \left[\frac{v_{\alpha}}{|v_{\beta}|} \right]^{1/2} r_{\alpha\beta} e^{-ik_{\beta} j a_L / 2} |j, \beta\rangle \right] + \sum_{j \geq N+1} \sum_{\beta} \left[\frac{v_{\alpha}}{|v_{\beta}|} \right]^{1/2} t_{\alpha\beta} e^{ik_{\beta} j a_L / 2} |j, \beta\rangle + \sum_{1 \leq j \leq N} \sum_{\kappa} \chi_{\alpha\kappa}^j |j, \kappa\rangle. \quad (3.7)$$

The incoming plane wave with wave number k_{α} may be reflected or transmitted with wave number k_{β} , with the restriction that the total energy and the parallel momentum are conserved. The velocity factors are included so that particle conservation yields a natural probabilistic interpretation of the transmission and reflection coefficients,

$$\sum_{\beta} [|t_{\alpha\beta}|^2 + |r_{\alpha\beta}|^2] = 1. \quad (3.8)$$

Information about the various tunneling states are contained in the coefficients $|\chi_{\alpha\kappa}^j|^2$, the j dependence of which yields the spatial-decay rate of the state with (in general) complex wave number k_{κ} . An expression for the transmission amplitude $t_{\alpha\beta}$ is obtained by comparing the projection $\{N+1, \beta|\Psi\rangle$ of Eqs. (3.1) and (3.7)

$$t_{\alpha\beta} = \left[\frac{v_{\beta}}{v_{\alpha}} \right]^{1/2} e^{-ik_{\beta}(N+1)a_L/2} \frac{4i\hbar}{a_L} \{N+1, \beta|G^{R\hat{v}}|0, \alpha\rangle. \quad (3.9)$$

In a similar way the projection $\{0, \beta|\Psi\rangle$ yields the reflection amplitude

$$r_{\alpha\beta} = \left[\frac{|v_{\beta}|}{v_{\alpha}} \right]^{1/2} \left[\frac{4i\hbar}{a_L} \{0, \beta|G^{R\hat{v}}|0, \alpha\rangle - \delta_{\alpha\beta} \{0_a, \alpha|0_a, \alpha\rangle \right], \quad (3.10)$$

where the second term comes from the fact that $|S_{\alpha}\rangle$ does not include the anion layer of site $j=0$. Equations (3.9) and (3.10) are readily seen to reduce to the expressions for $t(k)$ and $r(k)$ given in Eq. (2.9) of Ref. 30 for the simple case of a one-band 1D model.

Note that the ‘‘left’’ states $\{j, \beta|\}$ in (3.9) and (3.10) are not simply the Hermitian conjugate $\langle j, \beta|$ of $|j, \beta\rangle$. The reason is that the local projections $|j, \beta\rangle$ on a site j do not correspond to an orthogonal basis. Hence, $\langle j, \beta'|j, \beta\rangle \neq \delta_{\beta\beta'}$, and we must *construct* a new basis of left states such that $\langle j, \beta'|j, \beta\rangle = \delta_{\beta\beta'}$. Let B denote the 10×10 matrix whose columns are the ten states $|\beta\rangle \equiv |j, \beta\rangle$, independent of j . Then the matrix inverse B^{-1} is precisely the orthogonal basis that we need, with rows $\{\beta'|\}$. In addition to orthogonality one has, by con-

$$\hat{x} = \sum_j \left[|j_c\rangle \frac{j a_L}{2} (|j_c\rangle + |j_a\rangle) \left[\frac{j a_L}{2} + \frac{a_L}{4} \right] \langle j_a| \right]. \quad (3.6)$$

Here we have split the vector $|j\rangle$ into its cation and anion parts $|j_c\rangle$ and $|j_a\rangle$, respectively.

It is now straightforward to determine the scattering amplitudes. The total wave function may be written as

struction, the closure relations

$$\sum_{\beta} |\beta\rangle \langle \beta| = \sum_{\beta} |\beta\rangle \langle \beta| = 1. \quad (3.11)$$

We can bring Eqs. (3.9) and (3.10) into more symmetric forms by using the identity

$$\hat{v}|\alpha\rangle = v_{\alpha}|\alpha\rangle. \quad (3.12)$$

Here v_{α} is the velocity [in the (100) direction] associated with the state $|\alpha\rangle$. Equation (3.12) is a result of (B12) in Appendix B. Using (3.12) in (3.9) and (3.10) yields

$$T_{\alpha\beta} \equiv |t_{\alpha\beta}|^2 = \left| \frac{4i\hbar}{a_L} \sqrt{v_{\beta} v_{\alpha}} \{N+1, \beta|G^R|0, \alpha\rangle \right|^2, \quad (3.13)$$

$$R_{\alpha\beta} \equiv |r_{\alpha\beta}|^2 = \left| \frac{4i\hbar}{a_L} \sqrt{|v_{\beta}| v_{\alpha}} \{0, \beta|G^R|0, \alpha\rangle - \delta_{\alpha\beta} \{0_a, \alpha|0_a, \alpha\rangle \right|^2.$$

IV. ELECTRIC CURRENT

Transport in solids can be treated on various levels, depending on the approximations that are assumed at the outset. Examples are the semiclassical Boltzmann equation, the Kubo formula for linear response, and the Landauer formula which expresses the conductance of a system in terms of the single-particle transmission coefficients.³¹

In the case of a perfectly layered heterostructure it is well known that an expression for the electric current can be written down directly in terms of the transmission coefficients. Assume that one can define chemical potentials μ_L and μ_R in the left and right leads, respectively. Under equilibrium conditions $\mu_L = \mu_R$, and when a bias V is applied between the two leads, one has $\mu_R = \mu_L - eV$. Strictly speaking, these potentials do not describe the situation close to the barrier structure, a region that is out of equilibrium because of tunneling electrons. Thus, μ_L and μ_R correspond to asymptotic distributions in the leads. In the left lead, states with energy E are occupied with probability $f_{FD}(E - \mu_L) = [\exp\{(E - \mu_L)/k_B T]$

$+1]^{-1}$. Here f_{FD} is the Fermi-Dirac distribution function, k_B is Boltzmann's constant, and T is the temperature. An electron in initial state $|\alpha\rangle$ with velocity v_α in the (100) direction has probability $T_{\alpha\beta}$ of being transmitted into the right lead in a final state $|\beta\rangle$, which has probability $1 - f_{\text{FD}}(E - \mu_L + eV)$ of being empty. Analogous arguments hold for the states in the right lead. In order to find the total current flowing in the (100) direction, we must integrate over all possible states, i.e., over the Brillouin zone. In addition we have to sum over the different energy bands for each k .

In the present case, we have scattering processes that conserve parallel momentum and total energy, whereas the momentum $\hbar k$ in the (100) direction may be altered. It is, therefore, convenient to replace the integral over k and the sum over energy bands by an integral over energy and a sum over momenta $\hbar k_\alpha$:

$$\sum_n \int \frac{dk}{2\pi} = \sum_\alpha \int \frac{dE}{2\pi} \left[\frac{\partial E}{\partial k_\alpha} \right]^{-1}. \quad (4.1)$$

Since $(\partial E / \partial k_\alpha)^{-1} = (\hbar v_\alpha)^{-1}$, the total electric-current density is given by

$$J = -\frac{e}{\hbar} \sum_{\alpha\beta} \int \frac{dk_\parallel}{(2\pi)^2} \int \frac{dE}{2\pi} T_{\alpha\beta}(E, \mathbf{k}_\parallel) \times [f_{\text{FD}}(E - \mu_L) - f_{\text{FD}}(E - \mu_L + eV)]. \quad (4.2)$$

Here e is the absolute value of the electron charge so that $V > 0$ results in a net flow of electrons from left to right, i.e., a negative electric current. The sum over α and β is restricted to states with velocities $v_\alpha, v_\beta > 0$ in the (100) direction, and we have taken advantage of time-reversal symmetry under which $T(k_\alpha \rightarrow k_\beta) = T(-k_\beta \rightarrow -k_\alpha)$. The integral over parallel momentum \mathbf{k}_\parallel runs over the *two-dimensional Brillouin zone* which for the [100] plane in zinc-blende structures is a square with corners $(0, \pm 2\pi/a_L)$ and $(\pm 2\pi/a_L, 0)$.

Note that the simple arguments above are no longer applicable if one wants to include effects of alloy scattering or electron-phonon interactions. In that case a full Green-function treatment is required, and in Appendix B such an approach is presented. For the ideal case, where (4.2) is valid, we demonstrate explicitly the equivalence between the Green-function approach and the transmission-probability approach.

V. RESULTS AND DISCUSSION

The model and method described above can be applied to study electronic transport through arbitrary heterostructures with zinc-blende-type constituents. In this section, we shall concentrate on the ΓX mixing and transfer, and results will be presented exclusively for GaAs/AlAs heterostructures. We have used a simple, linear relation,

$$\Delta E_c^\Gamma(x) = 0.9x \text{ (eV)}, \quad (5.1)$$

for the Γ point conduction-band offset between $\text{Al}_x\text{Ga}_{1-x}\text{As}$ and GaAs. This is a compromise between

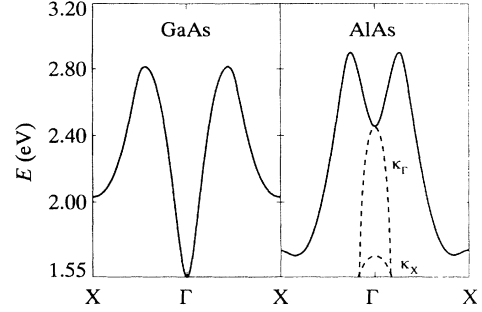


FIG. 2. Parts of the complex band structure for GaAs and AlAs. The solid lines are the lowest conduction band of the two materials. For AlAs we have also included the imaginary parts, κ_Γ and κ_X , of the analytical continuation below the minima at the Γ and X points, respectively. [To be precise, the conduction-band minimum of AlAs is not exactly at the X point in the present model, but slightly below, at $k \approx 0.85 \times (2\pi/a_L)$.] Zero energy is taken to be at the top of the valence band in GaAs, and with the present model and parameters GaAs has an energy gap of 1.55 eV.

various empirical relations quoted in the literature.³² In combination with the TB parameters of Ref. 24 (see Appendix A), Eq. (5.1) yields a discontinuity of about 0.16 eV between $E_c^X(\text{AlAs})$, i.e., the X point conduction-band minimum in AlAs, and $E_c^\Gamma(\text{GaAs})$. This is in agreement with recent experiments.⁷⁻⁹

We believe it is instructive to base the following discussion on parts of the *complex band structure* of GaAs and AlAs. In Fig. 2 the solid lines denote the lowest conduction band in the (100) direction, i.e., for $\mathbf{k}_\parallel = 0$. For AlAs we have also plotted the two branches of complex wave vector corresponding to the analytical continuation below the conduction-band minima at the Γ and X points of the Brillouin zone.³³ These branches are found by solving the Schrödinger equation for fixed energy E . In the present model there are ten solutions $k(E) = k_R + ik$ that make up the full complex band structure. In Fig. 2 we have only plotted the imaginary parts, κ_Γ and κ_X , of the two branches that are relevant to tunneling in a GaAs/AlAs heterostructure. For an incoming electron at energy E in the Γ valley of GaAs $\kappa_\Gamma(E)$ and $\kappa_X(E)$ determine the exponential decay of the tunneling wave functions ψ_Γ and ψ_X through the AlAs barrier(s). Clearly, the relative importance to the tunneling process of ψ_Γ and ψ_X will depend on which has the slowest decay in the barrier region. For energies below, but close to the conduction-band minima we have

$$\kappa_\Gamma(E) \simeq [2m_\Gamma^*(E_c^\Gamma - E)/\hbar^2]^{1/2}$$

and

$$\kappa_X(E) \simeq [2m_X^*(E_c^X - E)/\hbar^2]^{1/2},$$

where m_Γ^* and m_X^* are the effective masses in the Γ and the X valley, respectively. Thus, although the “ X barrier” $E_c^X - E$ is much lower than the “ Γ barrier” $E_c^\Gamma - E$, the large value of m_X^* yields $\kappa_X > \kappa_\Gamma$ for energies up to about 20 meV above the conduction-band minimum in GaAs. Furthermore, it is not only the exponential decay

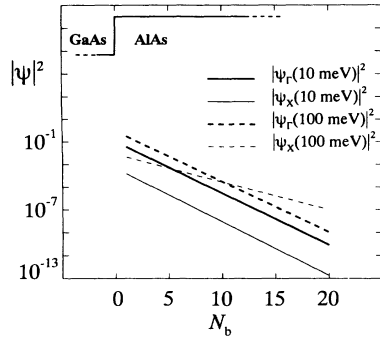


FIG. 3. Spatial decay into AlAs of the wave functions ψ_Γ (thick lines) and ψ_X (thin lines) at energies 10 meV (solid lines) and 100 meV (dashed lines) above the GaAs conduction-band edge $E_c^\Gamma(\text{GaAs})$. The distance from the GaAs/AlAs interface is given in terms of the number of AlAs monolayers N_b . The decay lengths corresponding to these curves are $\kappa_\Gamma^{-1} = 0.95a_L$ and $0.98a_L$; $\kappa_X^{-1} = 0.92a_L$ and $1.78a_L$. Here the first (second) number refers to the solid (dashed) lines, and $a_L = 5.66 \text{ \AA}$ is the lattice constant in AlAs. The inset illustrates the Γ point conduction-band minimum which represents a potential step between $N_b = 0$ and $N_b = 1$. The wave functions are normalized to an incoming plane wave of unit amplitude (see Sec. III).

of the tunneling wave functions that determine their contribution to transmission through a barrier. At the material interfaces plane waves in GaAs must be matched to the wave functions ψ_Γ and ψ_X in the AlAs barrier. From symmetry arguments we expect, for an incoming Γ electron, a larger matrix element for the matching to ψ_Γ than to ψ_X . These effects are illustrated in Fig. 3 where we have plotted the absolute value of the tunneling states as a function of position for a GaAs/AlAs potential step. The solid lines represent states at an energy 10 meV above $E_c^\Gamma(\text{GaAs})$. The stronger coupling to ψ_Γ is clearly observed by the fact that $|\psi_\Gamma| \gg |\psi_X|$ in the first layer of AlAs (i.e., for $N_b = 1$). Furthermore, since $\kappa_X \gtrsim \kappa_\Gamma$ for this energy, ψ_X decays slightly faster than ψ_Γ , and tunneling will predominantly happen via ψ_Γ . At an energy of 100 meV above $E_c^\Gamma(\text{GaAs})$ (dashed lines) we see again the stronger coupling to ψ_Γ at the material interface. However, in this case κ_X is considerably smaller than κ_Γ , and beyond the tenth AlAs monolayer we have $|\psi_X| > |\psi_\Gamma|$. Thus, depending on the width of the AlAs barrier, tunneling at this energy may take place via ψ_Γ , ψ_X , or both.

In a typical experiment the Fermi level is about 10–50 meV above $E_c^\Gamma(\text{GaAs})$. With the aid of Fig. 4 we will now sketch a qualitative picture of the tunneling of an electron through a single AlAs barrier, where a bias V is applied such that transfer to the GaAs X valley is possible. Let us assume that the energy of the electron is far from any resonances in the system. At the left interface (x_1) the matching of the incoming plane wave to tunneling states ψ_Γ and ψ_X may be described with matrix elements $M_{\Gamma\Gamma}(x_1)$ and $M_{\Gamma X}(x_1)$, respectively. We saw in Fig. 3, in accordance with expectations, that $M_{\Gamma\Gamma} \gg M_{\Gamma X}$. Since there is a bias across the barrier, the decay parameters κ_Γ and κ_X will now be functions of position within the barrier. Between x_1 and x_2 (typically a very short

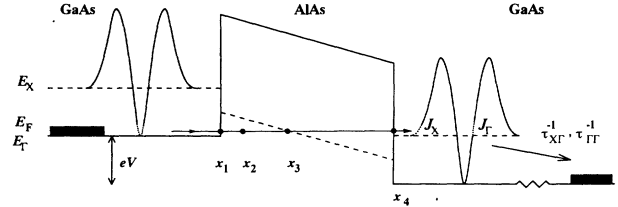


FIG. 4. Tunneling of an electron through a single AlAs barrier with applied bias V . The profiles of the Γ and X point conduction-band minima are represented by the solid and dashed lines, respectively. The lowest conduction band in GaAs [in the (100) direction] is sketched on both sides of the barrier, and the dotted portions indicate initially occupied states on the left side and available transmission states on the right side. Shaded areas denote the filled equilibrium Fermi sea in the emitter and collector contact. The transmitted electron may contribute to the “direct” current density J_Γ or the “transferred” one J_X . The tunneling process is described in detail in the text. Relaxation processes that bring the transmitted electrons to thermal equilibrium are indicated with scattering rates $\tau_{\Gamma\Gamma}^{-1}$ and $\tau_{X\Gamma}^{-1}$.

distance), we have $\kappa_X > \kappa_\Gamma$, so up to this point tunneling via ψ_Γ dominates strongly. However, beyond x_2 we have $\kappa_X < \kappa_\Gamma$, and the amplitude for tunneling via ψ_X is “catching up” relative to that of ψ_Γ . Between x_3 and x_4 the energy of the tunneling electron lies above $E_c^X(\text{AlAs})$. This means that $\kappa_X = 0$, and the amplitude of ψ_X is not further reduced whereas ψ_Γ continues to decay exponentially. Finally, at the right interface (x_4) matching of the two tunneling states to transmitted states in the collector contact may be described by matrix elements $M_{\alpha\beta}(x_4)$, with $\alpha, \beta = \Gamma$ or X . As above we expect the coupling between states of different symmetry ($M_{\Gamma X}$ and $M_{X\Gamma}$) to be much weaker than that between “similar” states ($M_{\Gamma\Gamma}$ and M_{XX}).

Based on this simple picture we can make predictions concerning the two contributions, J_Γ and J_X , to the total current density in a GaAs/AlAs heterostructure. First, there is no ΓX transfer for biases $V < [E_c^X(\text{GaAs}) - E_F]/e$. However, the direct component J_Γ may still be strongly affected by the presence of the tunneling state ψ_X , in particular due to resonant tunneling via confined X states in the barrier. We will briefly come back to this below. For biases $V > [E_c^X(\text{GaAs}) - E_F]/e$, ΓX transfer is possible, and the total current density is given by the sum of J_Γ and J_X . Their relative contribution is determined by two competing factors. On one hand, J_Γ is favored by the stronger coupling to ψ_Γ at the barrier interface. On the other hand, J_X is favored by the slower exponential decay of ψ_X through the barrier. For very thin barriers the interface coupling is the decisive factor, and we expect $J_\Gamma > J_X$. With increasing thickness of the barrier the difference in decay rate will eventually yield $J_X > J_\Gamma$, and the crossover to a “ ΓX filter” takes place around a barrier width $L_{\Gamma X}$ that will be estimated below via numerical examples.

The qualitative discussion above can only be expected to be valid in the off-resonant tunneling regime. The resonant features of tunneling through indirect-band-gap

heterostructures have been discussed extensively in the literature,^{17,18} and they have been observed very clearly in experiments.^{8,10} In general there are two types of resonant states in a GaAs/AlAs structure. With two or more AlAs barriers there will be one or more GaAs wells in which one finds the “normal” quasibound states ε_Γ confined by the Γ profile of the conduction band. On the other hand, the X profile of the conduction band reverses the role of barrier and well material, and as a result there will be resonant levels ε_X confined to the AlAs layers. These states are degenerate with the continuum of the GaAs contacts and hence similar to the so-called Fano resonances in atomic physics.³⁴ Predictions concerning resonance positions and linewidths are to some extent model dependent, as discussed in Ref. 18. Here we shall not elaborate further on the resonant structure of the current, although tunneling via resonant levels is indeed taking place in the structures studied below (*only* ε_X in the single-barrier case, *both* ε_Γ and ε_X in the double-barrier case).

In order to determine the conditions for having a ΓX filter, we have calculated current-voltage curves for a number of single- and double-barrier structures. Explicit results will be shown for single barriers only. We have used a Fermi level of 10 meV above the GaAs conduction-band edge. Furthermore, the potential profile is taken to be flat throughout the GaAs contacts, with a linear voltage drop across the barrier structure. In Fig. 5 we have plotted the two current-density components J_Γ (thick solid line) and J_X (thick dashed line) for a single AlAs barrier of width 40 Å, for biases in the range where ΓX transfer is possible,³⁵ and at zero temperature. We have also included the corresponding transmission coefficients T_Γ (thin solid line) and T_X (thin dashed line) at the Fermi level and with $\mathbf{k}_\parallel=0$. This shows that, although J_Γ and J_X are given by integrals over E and \mathbf{k}_\parallel of T_Γ and T_X , respectively, their dependence on applied bias is to a very good approximation reflected in a *single value* of the transmission coefficient. Of course, the in-

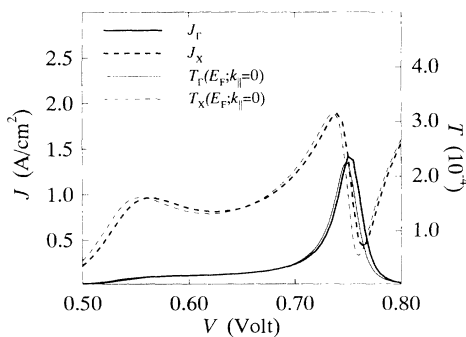


FIG. 5. Direct and transferred current-density contributions (thick lines), J_Γ and J_X , for a single AlAs barrier of width 40 Å. The corresponding transmission coefficients (thin lines), T_Γ and T_X , at $E = E_F = 10$ meV and $\mathbf{k}_\parallel = 0$ reflect to a good approximation both the qualitative behavior of J_Γ and J_X , and also their relative contributions to the total current density. The left vertical axis represents J_Γ and J_X in A/cm²; the right axis represents T_Γ and T_X which are of the order of 10^{-4} in this case.

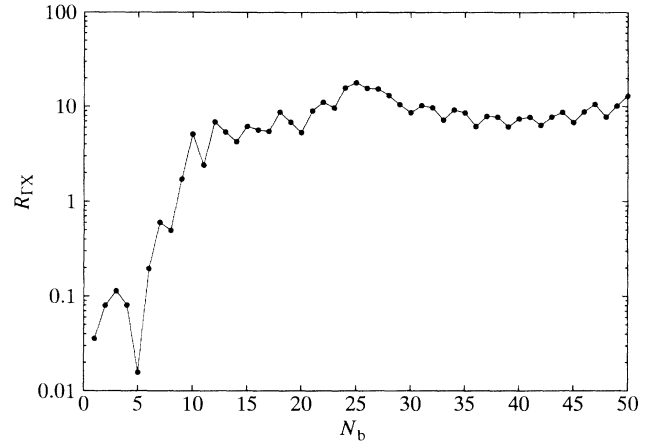


FIG. 6. $R_{\Gamma X}$, as defined in Eq. (5.2), for a single AlAs barrier as a function of barrier width, the latter given in terms of N_b , the number of monolayers of AlAs. The solid line connecting the data points is nothing more than a guide to the eye. $R_{\Gamma X}$ gives a quantitative measure of the relative contribution of J_X and J_Γ to the total current density: $R_{\Gamma X} \ll 1$ implies negligible ΓX transfer; $R_{\Gamma X} \gg 1$ implies large ΓX transfer.

tegrals over E and \mathbf{k}_\parallel tend to give a smoother behavior of $J(V)$ than that of $T(V)$. In addition, resonance positions and relative peak values may be slightly shifted in $J(V)$ when compared with $T(V)$. However, since we are not interested in details in the current-voltage curves, the following discussion may be based on the behavior of T_Γ and T_X at $E = E_F$ and $\mathbf{k}_\parallel = 0$.

From Fig. 5 we see that a single AlAs barrier acts like a good ΓX filter for a width of 40 Å. As a measure of the ΓX transfer we have calculated the ratio

$$R_{\Gamma X} \equiv \frac{\int dV T_X(V; E = E_F; \mathbf{k}_\parallel = 0)}{\int dV T_\Gamma(V; E = E_F; \mathbf{k}_\parallel = 0)}, \quad (5.2)$$

with limits of integration at 0.5 and 0.8 V.³⁶ The result is shown in Fig. 6 where $R_{\Gamma X}$ is plotted versus the number of monolayers of AlAs in the barrier. As expected there is only negligible ΓX transfer for very narrow barriers, but already at 10 monolayers there is almost an order of magnitude more electrons being transmitted in the X valley than in the Γ valley. Hence, the single AlAs barrier behaves like a ΓX filter with a crossover thickness $L_{\Gamma X} \sim 25$ Å.

We have also performed analogous calculations for double-barrier structures. As mentioned above, a qualitative difference from the single-barrier case is that resonant tunneling may happen not only via confined X states in the barriers, but also via confined Γ states in the well. Hence the resulting current-voltage curves display more resonances, both asymmetric Fano resonances and “normal” resonances with a Breit-Wigner form.

Because of the complicated resonant behavior of T_Γ and T_X , $R_{\Gamma X}$ is not a smoothly increasing function of barrier width. This is already apparent in Fig. 6, and in the case of a double barrier the oscillations are even stronger. Even so it is possible to distinguish two regimes, one where mostly $R_{\Gamma X} \ll 1$ and another where

mostly $R_{\Gamma X} \gg 1$. For the double-barrier structure we have evaluated $R_{\Gamma X}$ as a function of AlAs barrier width, for four different GaAs well widths: 6, 17, 34, and 56 Å. The resulting barrier crossover widths are $L_{\Gamma X} \sim 14, 22, 25,$ and 25 Å, respectively. This result can be understood as follows. When the well is very narrow and consists of only two monolayers of GaAs, there is strong coupling between the X states in each barrier. Hence the crossover width for one barrier is about half the crossover width in the single-barrier case. With increasing well width the coupling between the X states in each barrier becomes weaker, and $L_{\Gamma X}$ approaches the value found in the single-barrier case.

VI. CONCLUSIONS

We have presented a framework for the study of tunneling in III-V semiconductor heterostructures. A multi-band tight-binding model was used to obtain a realistic description of the lowest conduction band of each material. We applied the model to GaAs/AlAs structures where the barrier material has an indirect band gap. Tunneling states ψ_{Γ} and ψ_X contribute to transmission. For barriers wider than about ten monolayers of AlAs, tunneling via ψ_X dominates. An applied bias larger than, in the present model, 0.5 V enables transfer of Γ electrons to the X valley in GaAs. The ΓX transfer is stimulated by an indirect-band-gap AlAs barrier. With a conduction-band offset of 160 meV between GaAs and AlAs we find a barrier ‘‘crossover width’’ $L_{\Gamma X} \sim 25$ Å which separates a regime of negligible ΓX transfer (narrow barriers) from a regime of large ΓX transfer (wide barriers).

Finally, we would like to comment that the present model is quite general. Given the crystal structure, a set of tight-binding parameters, and the conduction-band offsets between the materials involved, one can study transport through structures of arbitrary composition. Interesting applications, besides the one studied here, could be the polytype type-II heterostructures³⁷ and the mixing of hole states in a pn junction. One might also try to apply the model on the level of the coherent-potential

approximation, first, to enable a study of the effects of alloy scattering in, e.g., $\text{Al}_x\text{Ga}_{1-x}\text{As}$, and second, to see how interface roughness affects the ΓX transfer.

ACKNOWLEDGMENTS

This work was supported in part by Norges Forskningsråd.

APPENDIX A

From Eq. (2.1) we have

$$(nbj\mathbf{k}_{\parallel}|H|n'b'j'\mathbf{k}_{\parallel}) = L_{\text{BZ}}^{-1} \int dk_x e^{ik_x(j-j')a_L/4} \times (nb\mathbf{k}|H|n'b'\mathbf{k}), \quad (\text{A1})$$

where the matrix elements $(nb\mathbf{k}|H|n'b'\mathbf{k})$ are given in Table A of Ref. 24. For example, the matrix element between the anion s orbital and the cation p_z orbital is

$$(sa\mathbf{k}|H|p_z c\mathbf{k}) = V(sa, pc)g_3(\mathbf{k}). \quad (\text{A2})$$

Here $V(sa, pc) = 4(sa\mathbf{R}_a|H|pc\mathbf{R}_c)$ is one of the, thirteen in all, independent TB matrix elements in the basis of symmetrically orthogonalized atomic orbitals $|nb\mathbf{R})$, and $g_3(\mathbf{k})$ may be regarded as a form factor that is determined by the symmetry of the crystal.²⁶ One may write

$$g_3(\mathbf{k}) = e^{ik_x a_L/4} \frac{i}{2} \text{sink}_{\parallel} \cdot \mathbf{d}_1 - e^{-ik_x a_L/4} \frac{i}{2} \text{sink}_{\parallel} \cdot \mathbf{d}_2, \quad (\text{A3})$$

where $\mathbf{d}_1 = (1, 1)a_L/4$ and $\mathbf{d}_2 = (1, -1)a_L/4$ are vectors in the (y, z) plane. Hence (A1) readily yields

$$(saj\mathbf{k}_{\parallel}|H|p_z c j'\mathbf{k}_{\parallel}) = V(sa, pc) \left[\delta_{j+1, j'} \frac{i}{2} \text{sink}_{\parallel} \cdot \mathbf{d}_1 - \delta_{j-1, j'} \frac{i}{2} \text{sink}_{\parallel} \cdot \mathbf{d}_2 \right] \quad (\text{A4})$$

for the matrix element in the desired basis. In Eq. (2.2) we let U_{ac} represent the ‘‘hopping’’ from an anion layer j to a cation layer $j-1$, whereas V_{ac} represents the hopping in the other direction, from j to $j+1$.³⁸ We then have, with $s_n \equiv \frac{1}{2} \text{sink}_{\parallel} \cdot \mathbf{d}_n$ and $c_n \equiv \frac{1}{2} \text{cosk}_{\parallel} \cdot \mathbf{d}_n$ ($n=1, 2$), the following elements of our Hamiltonian:

$$E_b = \begin{bmatrix} E(s, b) & & & & \\ & E(p, b) & & & \\ & & E(p, b) & & \\ & & & E(p, b) & \\ & & & & E(s^*, b) \end{bmatrix} \quad b = c \text{ or } a, \quad (\text{A5})$$

$$U_{ac} = \begin{bmatrix} V(s, s)c_2 & -V(sa, pc)c_2 & iV(sa, pc)s_2 & -iV(sa, pc)s_2 & 0 \\ V(pa, sc)c_2 & V(x, x)c_2 & -iV(x, y)s_2 & iV(x, y)s_2 & V(pa, s^*c)c_2 \\ -iV(pa, sc)s_2 & -iV(x, y)s_2 & V(x, x)c_2 & -V(x, y)c_2 & -iV(pa, s^*c)s_2 \\ iV(pa, sc)s_2 & iV(x, y)s_2 & -V(x, y)c_2 & V(x, x)c_2 & iV(pa, s^*c)s_2 \\ 0 & -V(s^*a, pc)c_2 & iV(s^*a, pc)s_2 & -iV(s^*a, pc)s_2 & V(s^*, s^*)c_2 \end{bmatrix},$$

$$V_{ac} = \begin{pmatrix} V(s,s)c_1 & V(sa,pc)c_1 & iV(sa,pc)s_1 & iV(sa,pc)s_1 & 0 \\ -V(pa,sc)c_1 & V(x,x)c_1 & iV(x,y)s_1 & iV(x,y)s_1 & -V(pa,s^*c)c_1 \\ -iV(pa,sc)s_1 & iV(x,y)s_1 & V(x,x)c_1 & V(x,y)c_1 & -iV(pa,s^*c)s_1 \\ -iV(pa,sc)s_1 & iV(x,y)s_1 & V(x,y)c_1 & V(x,x)c_1 & -iV(pa,s^*c)s_1 \\ 0 & V(s^*a,pc)c_1 & iV(s^*a,pc)s_1 & iV(s^*a,pc)s_1 & V(s^*,s^*)c_1 \end{pmatrix}.$$

In addition $U_{ca} = U_{ac}^\dagger$ and $V_{ca} = V_{ac}^\dagger$. Numerical values for GaAs and AlAs, taken from Ref. 24, are collected in Table I.

APPENDIX B

In this appendix, we will follow a general approach and obtain the electric-current density in terms of nonequilibrium Green functions. Using so-called “surface Green functions” we will show how to make contact with the transmission-probability approach presented in Sec. IV. The present treatment is closely related to the one introduced by Caroli *et al.*³⁹ For a system of noninteracting electrons, the total current density J is given in terms of the single-particle current-density operator \hat{J} as a many-body *quantum* average over occupied single-particle states, and a *statistical* average over all possible many-body configurations. Thus,

$$J = \sum_{\{m\}} P(m) \sum_s p_m(s) \langle \phi_s | \hat{J} | \phi_s \rangle, \quad (\text{B1})$$

where $P(m)$ is the probability of having the many-body configuration $\{m\}$, and $p_m(s)$ is the probability that the single-particle state $|\phi_s\rangle$ is occupied in the given many-body configuration [$p_m(s)$ equals 0 or 1]. Since the *reduced density matrix* ρ is defined as

$$\rho = \sum_{\{m\}} P(m) \sum_s p_m(s) |\phi_s\rangle \langle \phi_s|, \quad (\text{B2})$$

we may also write

$$J = \text{tr}(\rho \hat{J}), \quad (\text{B3})$$

where tr denotes the trace operation. The connection to Green functions is now transparent since

$$\rho = \int \frac{dE}{2\pi} G^<(E), \quad (\text{B4})$$

where we follow the notation in, e.g., Ref. 40. The *correlation* function $G^<$ and its hole “counterpart” $G^>$ are re-

lated to the *retarded* and *advanced* Green functions G^R and G^A via⁴⁰

$$G^< + G^> = i(G^R - G^A). \quad (\text{B5})$$

In general only two of the four functions in (B5) are independent since one also has the connecting identity

$$G^R = [G^A]^\dagger. \quad (\text{B6})$$

Equations (B3)–(B6) constitute the proper starting point for evaluation of the electric-current density in a system of noninteracting electrons.

An operator \hat{J} for the electric-current density is found by comparing the continuity equation and the Heisenberg equation of motion. We also use (B4) and obtain the result

$$J_{m,m+1} = -\frac{e}{\hbar} \int \frac{dE}{2\pi} \int \frac{d\mathbf{k}_\parallel}{(2\pi)^2} i \text{tr}(G_{m+1,m}^< u_{m,m+1} - G_{m,m+1}^< u_{m+1,m}) \quad (\text{B7})$$

for the net current density flowing between layers m and $m+1$ (in the positive x direction). In (B7) the matrix elements of $G^<$ depend, of course, on E and \mathbf{k}_\parallel , and the TB “hopping” elements $u_{m,m\pm 1}$ depend on \mathbf{k}_\parallel in a way that is determined by the crystal structure (see Appendix A). Equation (B7) is valid for systems that have translational invariance in the parallel plane and are characterized by a nearest-neighbor TB Hamiltonian.

In order to connect the Green-function approach and the transmission-probability approach, we must show that

$$\begin{aligned} i \text{tr}(G_{m+1,m}^< u_{m,m+1} - G_{m,m+1}^< u_{m+1,m}) \\ = \sum_{\alpha\beta} T_{\alpha\beta} [f_{\text{FD}}(E - \mu_L) - f_{\text{FD}}(E - \mu_L + eV)] \end{aligned} \quad (\text{B8})$$

when we have a structure connected to semi-infinite perfect leads in equilibrium at chemical potentials μ_L and

TABLE I. Empirical matrix elements of the sp^3s^* Hamiltonian in eV for GaAs and AlAs.

Compound	$E(s,a)$	$E(p,a)$	$E(s,c)$	$E(p,c)$	$E(s^*,a)$	$E(s^*,c)$	$V(s,s)$
GaAs	-8.3431	1.0414	-2.6569	3.6686	8.5914	6.7386	-6.4513
AlAs	-7.5273	0.9833	-1.1627	3.5867	7.4833	6.7267	-6.6642
Compound	$V(x,x)$	$V(x,y)$	$V(sa,pc)$	$V(pa,sc)$	$V(s^*a,pc)$	$V(pa,s^*c)$	$V(s^*,s^*)$
GaAs	1.9546	5.0779	4.4800	5.7839	4.8422	4.8077	0.0000
AlAs	1.8780	4.2919	5.1106	5.4965	4.5216	4.9950	0.0000

$\mu_R = \mu_L - eV$. The following ingredients are required to rewrite the left-hand side of this equation:

(1) The equilibrium expressions for $G^<$ and $G^>$ in a homogeneous system at chemical potential μ :⁴¹

$$\begin{aligned} g^<(E) &= i[g^R(E) - g^A(E)]f_{\text{FD}}(E - \mu), \\ g^>(E) &= i[g^R(E) - g^A(E)][1 - f_{\text{FD}}(E - \mu)]. \end{aligned} \quad (\text{B9})$$

(We use lowercase letters for Green functions that describe a system in equilibrium.)

(2) The rules, derived by Langreth and Wilkins,⁴² for handling products of two or more Green functions

$$\begin{aligned} (AB)^R &= A^R B^R, \\ (AB)^A &= A^A B^A, \\ (AB)^< &= A^R B^< + A^< B^A, \\ (AB)^> &= A^R B^> + A^> B^A. \end{aligned} \quad (\text{B10})$$

(3) The Dyson equation and the recursive Green-function technique, described in detail in the Appendix of Ref. 30.

(4) The unit matrices of Eq. (3.11).

Straightforward algebra then yields

$$\begin{aligned} &\sum_{\alpha\beta\mu\nu} (\alpha_c | U_{ca} 2 \text{Im}\gamma_a^+ U_{ac} | \beta_c) \{ \beta | G_{N+1,0}^R | \mu \} \\ &\times (\mu_a | U_{ac} 2 \text{Im}\gamma_c^- U_{ca} | \nu_a) \{ \nu | G_{0,N+1}^A | \alpha \} \\ &\times [f_{\text{FD}}(E - \mu_L) - f_{\text{FD}}(E - \mu_L + eV)] \end{aligned} \quad (\text{B11})$$

for the left-hand side of (B8), where we have chosen to let the cation and anion layers of “site” $N + 1$ represent m and $m + 1$, respectively. Here subscripts c or a on the states α , β , μ , and ν denote the cation or anion parts, respectively. Further, $2 \text{Im}\gamma \equiv i(\gamma^A - \gamma^R)$,⁴³ and γ_a^+ (γ_c^-) is the surface Green function, i.e., the local element at the surface layer of the Green function for a semi-infinite crystal extending from layer $N + 1, a(0, c)$ to $+\infty(-\infty)$. Remember, sites $N + 1$ and 0 are defined as the first sites of the semi-infinite crystals at *constant* potential energy on each side of the heterostructure. From the recurrent relations for the surface Green functions³⁰ it is clear that γ_a^+ is the same on site $N + 1$ as in $+\infty$, and γ_c^- the same on site 0 as in $-\infty$. In other words, γ_a^+ and γ_c^- in (B11)

reflect asymptotic properties of the left and right lead, respectively, which allows for the use of (B9) in deriving (B11).

In (B11) only a few terms contribute to the sum. First, there can only be a contribution from *extended* states with real values of k . Clearly, the result of (B11) must be unchanged if we choose sites, other than $N + 1$ and 0 , further into the asymptotic regions. However, *evanescent* states β or μ would give a modulus $|\{\beta | G_{ij}^R | \mu\}|$ that decreases exponentially with increasing i or decreasing j ($i \geq N + 1, j \leq 0$). Second, only states with *positive* velocity contribute to the sum since the *retarded* Green function propagates a scattering state forward in time. Finally, since $G^A = [G^R]^\dagger$, the states ν and α must also be extended states with positive velocities.

What remains is to evaluate the matrix elements $(\alpha_c | U_{ca} 2 \text{Im}\gamma_a^+ U_{ac} | \beta_c)$ and $(\mu_a | U_{ac} 2 \text{Im}\gamma_c^- U_{ca} | \nu_a)$. This task is accomplished by rewriting matrix elements of the velocity operator \hat{v} [see Eq. (3.5)] with the help of the Dyson equation and the recursive Green-function technique. The result is

$$\begin{aligned} (\alpha_c | U_{ca} 2 \text{Im}\gamma_a^+ U_{ac} | \beta_c) &= -\frac{4\hbar}{a_L} (\alpha | \hat{v} | \beta) \\ &= -\frac{4\hbar}{a_L} v_\alpha \delta_{\alpha\beta}, (v_\alpha > 0), \end{aligned} \quad (\text{B12})$$

$$\begin{aligned} (\mu_a | U_{ac} 2 \text{Im}\gamma_c^- U_{ca} | \nu_a) &= \frac{4\hbar}{a_L} (\mu | \hat{v} | \nu) = \frac{4\hbar}{a_L} v_\mu \delta_{\mu\nu}, \\ &(v_\mu < 0). \end{aligned}$$

Here the relation $(\alpha | \hat{v} | \beta) = v_\alpha \delta_{\alpha\beta}$ follows from current conservation. Although states with negative velocity do not contribute to the sum in (B11), there corresponds to each state μ (with $v_\mu < 0$) a “time-reversed” state μ' (with $v_{\mu'} = -v_\mu > 0$) for which one has⁴⁴

$$(\mu'_a | U_{ac} 2 \text{Im}\gamma_c^- U_{ca} | \mu'_a) = -\frac{4\hbar}{a_L} v_{\mu'}. \quad (\text{B13})$$

Finally, collecting all our knowledge, the sum in (B11) may be written as

$$\begin{aligned} &\sum_{\alpha\beta\mu\nu} \frac{4\hbar}{a_L} v_\alpha \delta_{\alpha\beta} \{ \beta | G_{N+1,0}^R | \alpha \} \frac{4\hbar}{a_L} v_\mu \delta_{\mu\nu} \{ \nu | G_{0,N+1}^A | \alpha \} [f_{\text{FD}}(E - \mu_L) - f_{\text{FD}}(E - \mu_L + eV)] \\ &= \sum_{\alpha\beta} \left[\frac{4\hbar}{a_L} \right]^2 v_\alpha v_\beta |\{ \beta | G_{N+1,0}^R | \alpha \}|^2 [f_{\text{FD}}(E - \mu_L) - f_{\text{FD}}(E - \mu_L + eV)] \\ &\equiv \sum_{\alpha\beta} T_{\alpha\beta} [f_{\text{FD}}(E - \mu_L) - f_{\text{FD}}(E - \mu_L + eV)], \end{aligned} \quad (\text{B14})$$

which demonstrates the validity of Eq. (B8), and hence the equivalence of the transmission-probability approach in Sec. IV and the Green-function approach.

- *Present address: Institutt for Fysikk, Norges Tekniske Høgskole, Universitetet i Trondheim, N-7034 Trondheim-NTH, Norway.
- ¹I. Hase *et al.*, *J. Appl. Phys.* **59**, 3792 (1986).
- ²E. E. Mendez, E. Calleja, and W. I. Wang, *Phys. Rev. B* **34**, 6026 (1986).
- ³N. R. Couch *et al.*, *Semicond. Sci. Technol.* **2**, 244 (1987).
- ⁴E. E. Mendez *et al.*, *Appl. Phys. Lett.* **50**, 1263 (1987).
- ⁵M. S. Skolnick *et al.*, *Phys. Rev. B* **39**, 11 191 (1989).
- ⁶A. J. Shields *et al.*, *Phys. Rev. B* **42**, 5879 (1990).
- ⁷S. S. Lu *et al.*, *J. Appl. Phys.* **67**, 6360 (1990).
- ⁸R. Pritchard *et al.*, *J. Appl. Phys.* **68**, 205 (1990).
- ⁹S. S. Lu, M. I. Nathan, and C. C. Meng, *J. Appl. Phys.* **69**, 525 (1991).
- ¹⁰D. G. Austing *et al.*, *Phys. Rev. B* **47**, 1419 (1993).
- ¹¹N. A. Cade *et al.*, *Solid State Commun.* **64**, 283 (1987).
- ¹²H. C. Liu, *Appl. Phys. Lett.* **51**, 1019 (1987).
- ¹³J.-B. Xia, *Phys. Rev. B* **41**, 3117 (1990).
- ¹⁴M. Rossmannith, J. Leo and K. von Klitzing, *J. Appl. Phys.* **69**, 3641 (1991).
- ¹⁵T. F. Zheng *et al.*, *J. Appl. Phys.* **69**, 8387 (1991).
- ¹⁶V. Sankaran and J. Singh, *Phys. Rev. B* **44**, 3175 (1991).
- ¹⁷P. A. Schulz, *Phys. Rev. B* **44**, 8323 (1991).
- ¹⁸D. Z.-Y. Ting and T. C. McGill, *Phys. Rev. B* **47**, 7281 (1993).
- ¹⁹Including various scattering mechanisms, but still with noninteracting electrons.
- ²⁰S. Adachi, *J. Appl. Phys.* **58**, R1 (1985).
- ²¹W. Fawcett, A. D. Boardman, and S. Swain, *J. Phys. Chem. Solids* **31**, 1963 (1970).
- ²²B. K. Ridley, *Quantum Processes in Semiconductors* (Oxford, New York, 1982).
- ²³This is, for example, the case for shot noise in Coulomb-blockade systems; see U. Hanke *et al.* (unpublished).
- ²⁴P. Vogl, H. P. Hjalmarson, and J. D. Dow, *J. Phys. Chem. Solids* **44**, 365 (1983).
- ²⁵E. Yamaguchi, *J. Phys. Soc. Jpn.* **56**, 2835 (1987).
- ²⁶W. A. Harrison, *Electronic Structure and the Properties of Solids* (Freeman, San Francisco, 1980).
- ²⁷D. J. Chadi and M. L. Cohen, *Phys. Status Solidi* **68**, 405 (1975).
- ²⁸P. O. Löwdin, *J. Chem. Phys.* **18**, 365 (1950).
- ²⁹See, for example, F. Sols *et al.*, *J. Appl. Phys.* **66**, 3892 (1989).
- ³⁰J. A. Støvneng and E. H. Hauge, *Phys. Rev. B* **44**, 13582 (1991).
- ³¹R. Landauer, *IBM J. Res. Dev.* **1**, 233 (1957); *Philos. Mag.* **21**, 863 (1970).
- ³²See, for example, S. Adachi, *J. Appl. Phys.* **58**, R1 (1985).
- ³³In the present model the conduction-band minimum in AlAs is not exactly at the X point, see Fig. 2.
- ³⁴U. Fano, *Phys. Rev.* **124**, 1866 (1961).
- ³⁵ ΓX transfer is also possible for biases above 0.8 V. However, the accuracy of the band structure in the sp^3s^* model diminishes at higher energies, and it seems reasonable to restrict the presentation to the lowest conduction band. In this model the second conduction band in GaAs starts at X_3^c , 0.83 eV above E_c^Γ .
- ³⁶These integration limits are chosen such that $R_{\Gamma X}$ reflects a sizable bias interval in which ΓX transfer is possible. At the same time we exclude from $R_{\Gamma X}$ the often large variations of T_Γ and T_X in the vicinity of the band edges X_1^c and X_3^c in the GaAs collector contact (i.e., $V \geq 0.47$ V and $V \leq 0.83$ V, respectively).
- ³⁷J. R. Söderström, D. H. Chow, and T. C. McGill, *Appl. Phys. Lett.* **55**, 1094 (1989).
- ³⁸Here, as well as in Sec. II, j labels individual atomic layers, in contrast to Sec. III where a common label is used for pairs of cation and anion layers.
- ³⁹C. Caroli *et al.*, *J. Phys. C* **4**, 916 (1971).
- ⁴⁰P. Lipavský, V. Špička, and B. Velický, *Phys. Rev. B* **34**, 6933 (1986).
- ⁴¹L. Kadanoff and G. Baym, *Quantum Statistical Mechanics* (Benjamin, New York, 1962).
- ⁴²D. Langreth and J. W. Wilkins, *Phys. Rev. B* **6**, 3189 (1972).
- ⁴³In general, only the *diagonal* elements of the resulting matrix $i(\gamma^A - \gamma^R)$ will actually be equal to two times the imaginary part of γ^R .
- ⁴⁴In general, γ^+ describes states with $v > 0$ or $\text{Im}k > 0$, whereas γ^- describes states with $v < 0$ or $\text{Im}k < 0$. The relation (B13) is found by inspection of the numerical results. It is probably related to time-reversal symmetry, but we have not been able to *derive* a relation that connects the matrix $U_{ac} 2 \text{Im} \gamma_c^- U_{ca}$ to states with positive velocity.

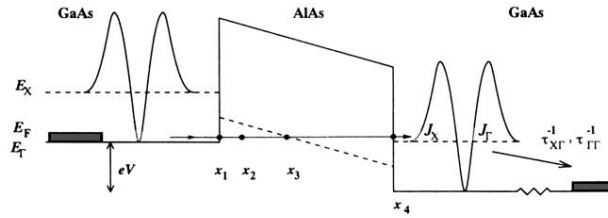


FIG. 4. Tunneling of an electron through a single AlAs barrier with applied bias V . The profiles of the Γ and X point conduction-band minima are represented by the solid and dashed lines, respectively. The lowest conduction band in GaAs [in the (100) direction] is sketched on both sides of the barrier, and the dotted portions indicate initially occupied states on the left side and available transmission states on the right side. Shaded areas denote the filled equilibrium Fermi sea in the emitter and collector contact. The transmitted electron may contribute to the “direct” current density J_{Γ} or the “transferred” one J_X . The tunneling process is described in detail in the text. Relaxation processes that bring the transmitted electrons to thermal equilibrium are indicated with scattering rates $\tau_{\Gamma\Gamma}^{-1}$ and $\tau_{X\Gamma}^{-1}$.